LA-UR-98-1237

Title: **One-Dimensional Time-to Explosion (ODTX) In HMX Spheres**

Author(s): W. Dale Breshears

Submitted to:

Los Alamos
NATIONAL LABORATORY
memorandum

Chemical Science and Technology
Responsible Chemistry for America

CST-6, MS J567
Los Alamos, New Mexico 87545

To/MS: Phil Howe, DX-DO, MS P915
From/MS: W. Dale Breshears, CST-6, MS J567
Phone/FAX: 5-7565/5-4817
Symbol: CST-6-U-97: 047
Date: June 2, 1997

ONE-DIMENSIONAL TIME-TO-EXPLOSION (ODTX) IN HMX SPHERES

1. Introduction

In a series of papers (Catalano *et al.*,[1] Paper 1; Tarver *et al.*,[2] Paper 2; McGuire and Tarver,[3] Paper 3; Tarver *et al.*,[4] Paper 4) researchers at Lawrence Livermore National Laboratory (LLNL) have reported measurements of the time to explosion in spheres of various high explosives following a rapid, uniform increase in the surface temperature of the sphere. Due to the spherical symmetry, the time-dependent properties of the explosive (temperature, chemical composition, etc.) are functions of the radial spatial coordinate only; thus the name "one-dimensional time-to-explosion" (ODTX).

The LLNL researchers also report an evolving series of computational modeling results for the ODTX experiments,[2-4] culminating in those obtained using a sophisticated heat transfer code incorporating accurate descriptions of chemical reaction.[5] Although the chemical reaction mechanism used to describe HMX decomposition is quite simple, the computational results agree very well with the experimental data, as shown here in Fig. 1. In addition to reproducing the magnitude and temperature dependence of the measured times to explosion, the computational results also agree with the results of post reaction visual inspection (see Section 2, below).

The ODTX experiments offer a near-ideal example of a transport process (heat transfer in this case) tightly coupled with chemical reaction. The LLNL computational model[4] clearly captures the important features of the ODTX experiments. An obvious question of interest is to what extent the model and/or its individual components (specifically the chemical reaction mechanism) are applicable to other experimental scenarios. Valid exploration of this question requires accurate understanding of (i) the experimental scenario addressed by the LLNL model and (ii) details of the application of the model. I report here recent work addressing points (i) and (ii).

2. ODTX Experiments

Experimental details given in Paper 1[1] are summarized here. Two aluminum anvils, each with a hemispherical cavity of radius equal to that of the spherical explosive sample machined into the face, are preheated to the desired temperature. By means of a vacuum chuck operated

remotely, the explosive sample is placed in the cavity of the lower anvil and the upper anvil is lowered to seal the sample cavity. A copper sealing ring between recessed knife edges machined in the anvil faces enables hydraulically applied *confinement* pressures up to 1500 atm to be achieved, although essentially no pressure is applied directly to the explosive sample. Sample insertion and anvil closing can be accomplished in approximately 0.6 s. Time is measured from anvil closing to an "endpoint" sensed by a microphone and an accelerometer mounted on the anvils.

Times thus measured for 1.27 cm diameter spheres of LX-10 (94.5% HMX plus 5.5% Viton A binder) are shown here in Fig. 1. The low temperature end of the data at 1000/T = 2.16 (T = 463 K) defines the "critical" temperature, *i.e.*, the temperature below which no measurable reaction violence is produced. From post reaction visual inspection of the anvils and the explosive sample, the authors of Paper 1[1] describe two distinct types of events.

> "A low order event, probably a rupture of the seals caused by gas pressure, yields little or no damage to the anvils; indeed the copper sealing ring is generally still in place and the majority of the explosive sample unconsumed though charred. . . . A high order event, on the other hand, causes considerable metal flow in the aluminum anvil and twisting and fragmentation of the copper seal."

In Paper 4[4] the authors report "the experimental observation that the degree of violence increases as the boundary temperature decreases and the time to explosion increases, allowing the heat to be transferred further into the LX-10 before explosion and thereby involving a greater mass of the explosive in the process."

3. The LLNL Computational Model

The most recent computational results reported by the LLNL researchers[4] were obtained using the "Chemical TOPAZ" code,[5] which allows each of many chemical species to be defined with its own thermal conductivity, heat capacity and heat of formation, and treats chemical reactions of any order between any subset of such species. It is important to note that the code is restricted to a system of constant volume and constant uniform mass density.[5]

Paper 4[4] points out that while the code is capable of treating a detailed reaction mechanism for HMX decomposition, uncertainties in the dominant reaction pathways and the relevant kinetic rate constants preclude such detail at present. The authors employ a mechanism comprising three reactions and four species, represented schematically as

HMX → "fragments" (R1)

"fragments" → "intermediate gases" (R2)

"intermediate gases" → "final gases." (R3)

Reaction R1 represents unimolecular endothermic breaking of C–C and/or C–N bonds in HMX ($C_4H_8N_8O_8$) to produce methylene nitramine ($CH_2N_2O_2$) and other fragments. Reaction R2 represents the weakly exothermic unimolecular decomposition of these fragments to produce gaseous intermediates: formaldehyde (CH_2O) plus N_2O and/or HCN plus HNO_2. Reaction R3 represents very exothermic bimolecular reactions between these gaseous intermediates to produce stable gaseous reaction products: H_2O plus CO plus N_2 and/or H_2 plus CO_2 plus N_2.

Table 1 of Paper 4,[4] reproduced here as Table 1, lists the thermal and chemical kinetic parameters used in the LLNL model for HMX (LX-10). The mass density given for HMX (1.865 g/cm^3) must, as noted above, remain constant and uniform throughout the volume. For each of the species defined above *i.e.*, HMX, fragments, intermediate gases ("gases 1") and final gases ("gases 2") thermal conductivities (cal/(cm-s-K)) and heat capacities (cal/g) are given as tabular functions of temperature along with the heat of formation at 298 K (cal/g). The lower part of the table gives Arrhenius parameters, reaction order, and heat of reaction at 298 K (cal/g) for reactions R1-R3. Arrhenius pre-exponential parameters are given in units of s^{-1} for all three reactions, including the *bimolecular* reaction R3, indicating that these rate constants do not apply to rate equations cast in the usual "chemical" terms of molar or molecular densities.

The code description[5] defines reaction rate expressions in terms of volume fractions, v_i, which, with constant uniform mass density, are equal to mass fractions, f_i. With indices 1-4 defining HMX, fragments, intermediate gases and final gases, respectively, the rate equations in mass fractions have the form

$$\frac{df_1}{dt} = -k_1 f_1 \; ; \qquad (1)$$

$$\frac{df_2}{dt} = k_1 f_1 - k_2 f_2 \; : \qquad (2)$$

$$\frac{df_3}{dt} = k_2 f_2 - k_3 f_3^2 \; ; \qquad (3)$$

$$\frac{df_4}{dt} = k_3 f_3^2 \; . \qquad (4)$$

Note that since in mass units, one gram of any given species is equivalent to one gram of any other species, the "stoichiometric" coefficients in Eqs. 1-4 are all unity.

Assigning chemical identities to species as suggested in Paper 4,[4] the reactions become

$C_4H_8N_8O_8 \rightarrow 4\, CH_2N_2O_2$; (R1')

$$CH_2N_2O_2 \rightarrow f_2\,(CH_2O+N_2O) + (1-f_2)\,(HCN+HNO_2)\,; \qquad \text{(R2')}$$

$$f_2\,(CH_2O+N_2O) + (1-f_2)\,(HCN+HNO_2) \rightarrow f_3\,(H_2O+CO+N_2) + (1-f_3)\,(H_2+CO_2+N_2)\,; \qquad \text{(R3')}$$

where f_2 and f_3 are branching fractions for the first product channels listed in reactions R2' and R3', respectively. Note that M_i, the average molecular weight of species i, is given by

$$M_i = \frac{M_1}{N_i}\ , \qquad (5)$$

where N_i is the number of moles of species i formed per mole of decomposition of species 1 (HMX). Thus N_i = 2, 8, 12 for i = 2, 3, 4, respectively.

At constant uniform mass density, molar densities, C_i, and mass fractions are related by

$$f_i = \frac{C_i M_i}{\rho}\ . \qquad (6)$$

Substitution of Eq. 6 in Eqs. 1-4 followed by substitution of Eq. 5 yields

$$\frac{dC_1}{dt} = -k'_1 C_1\,; \qquad (7)$$

$$\frac{dC_2}{dt} = 4k'_1 C_1 - k'_2 C_2\,; \qquad (8)$$

$$\frac{dC_3}{dt} = 2k'_2 C_2 - 2k'_3 C_3^2\,; \qquad (9)$$

$$\frac{dC_4}{dt} = 3\,k'_3 C_3^2\ . \qquad (10)$$

The primed and unprimed rate constants are related by

$$\frac{k_j}{k'_j} = n_j \left(\frac{N_i \rho}{M_1}\right)^{n-1}\ , \qquad (11)$$

where n_j is the order of reaction j and the index i refers to the reactant species for reaction j.

Since the ODTX experiments are performed in a constant volume system, the constant volume restriction, noted above, of the code used in the LLNL computations is not a problem.

The constant uniform density restriction is surely an approximation; however, the objective here, at least for the present, is to understand how the computational model is applied rather than to assess its validity.

4. Calculations with the LLNL Model

To test my understanding of the HMX reaction mechanism used by Tarver *et al.*[4] I have carried out computational simulations of the ODTX experiments using the parameter values given in Table 1. The equation describing coupled heat transfer and chemical reaction at constant volume is

$$\frac{1}{r^2}\frac{\partial}{\partial r}\left(\lambda r^2 \frac{\partial T}{\partial r}\right) + E' = \rho c_v \frac{\partial T}{\partial t} \quad . \tag{12}$$

Here r is the spherical radial coordinate, λ is thermal conductivity, T is temperature and ρ is density. Because of constant volume, E' is the net rate of change of *internal energy* per unit volume due to chemical reaction and c_v is the heat capacity at *constant volume.*

Table 1 gives heats (enthalpies) of formation and reaction. The heat capacities given for gases are much closer to values of c_p for the proposed chemical species than to those of c_v, and are assumed to be the former. For ideal gases

$$c_p = c_v + R \ , \tag{13}$$

and for condensed phase species

$$c_p \quad c_v \ . \tag{14}$$

The procedure for deriving the internal energy of formation from the heat (enthalpy) of formation is illustrated using HMX as an example. The first entry in Table 2 gives the overall reaction to form HMX from elements in their standard states. Noting that

$$H(\text{enthalpy}) = E(\text{internal energy}) + P(\text{pressure}) \times V(\text{volume}) \ , \tag{15}$$

we can derive

$$\Delta H^0_{HMX} = \Delta E^0_{HMX} + P\,(V_{HMX} - 4\,V_C) - 12\,RT \ , \tag{16}$$

where the ideal gas law, PV = RT is used for gaseous species. Assuming the term $P\,(V_{HMX} - V_C)$ for solids is always negligible relative to other terms on the right hand side of Eq. 16, that equation can be generalized for species i to the form

$$\Delta H^0_i = \Delta E^0_i + (\Delta N_{gi})\, RT\ , \qquad (17)$$

where ΔN_{gi} is the net change in number of moles of gaseous species in the overall formation reaction. Table 2 gives overall formation reactions and corresponding values of ΔN_g for the various choices of chemical species identified as fragments, intermediate gases ("Gases 1") and final gases ("Gases 2"). Note that each of the two sets of species for Gases 1 and Gases 2 yields the same average value of ΔN_g.

The heats of formation (cal/g) at 298 K in Table 1 were converted to molar units using molecular weights given by Eq. 5, molar internal energies of formation were calculated using Eq. 17, then converted back to units of mass (cal/g). Values of $\Delta E^0_i(T)$ were computed from the equation

$$\Delta E^0_i(T) = \Delta E^0_i(298) + \int_{298}^{T} c_{vi}\, dT'\ . \qquad (18)$$

Internal energies of reaction, $\Delta E^r_j(T)$, were computed from the $\Delta E^0_i(T)$. All temperature dependent quantities were evaluated using least-squares fits of linear or quadratic functions. Thermal conductivity was computed as the mass-weighted average of the individual species values.[5]

Equation 12 was integrated in time and radial coordinate using a scheme described by Becker[6] (pp. 110-112 and Appendix B). The radial grid comprised 21 points, with radial increments chosen to maintain spherical shells of constant volume. The radial grid point for each shell was at the volumetric center of the shell. The temperature of the outermost shell was held constant at $T = T_s$, the "surface" temperature of the anvils in the ODTX experiment. All other temperatures were set to T = 300 K at zero time. A variable integration time step was determined by computing a maximum temperature change, usually ΔT = 1 K, using the initial values of Eq. 16 for all grid points. Because the integration scheme averages radial derivatives over the integration time step, actual values of maximum ΔT varied from step to step. Integration was stopped when $(T_{max} - T_s) \geq 20$ K, where T_{max} is the maximum temperature at any radial grid point.

Calculations were performed using Microsoft Excel, Version 5.0a, in the iteration mode of calculation, on a Macintosh Powerbook 3400c/180 laptop computer. The number of iterations (each iteration corresponds to one integration time step) ranged from ~5000 at $1000/T_s = 1.80$ (556 K) to near 30000 at $1000/T_s = 2.14$ (467 K).

Results for the time to "explosion" as defined above are shown in Fig. 1 along with the experimental and computational results from Fig. 1 of Paper 4.[4] Given the coarseness of the radial grid and the generous time steps, the degree of agreement with the LLNL computational results is remarkable. The present calculations extend to $1000/T_s = 2.14$; at a value of 2.15,

(T_{max} - T_s) failed to reach 20 K before all radial temperatures began decreasing with time. Thus, the present calculations over predict the critical temperature by ~ 4 K.

Calculated radial profiles of temperature and HMX mass fraction at the time of "explosion" are shown for various temperatures in Figs. 2-5. These results agree with the qualitative experimental observations given in Papers 1[1] and 4. At the highest temperature reaction is confined to an outer radial shell. As the temperature decreases, the thickness of this shell increases until, at the lowest temperatures, the entire volume has reacted. Thus, as temperature decreases, reaction violence increases until the critical temperature is approached and a true thermal "explosion" ceases to occur in any part of the volume.

5. Summary and Conclusions

The reaction mechanism for HMX decomposition employed by Tarver *et al.*[4] in Paper 4 clearly captures the features important in the ODTX experiments. The good agreement of the rather crude (in the numerical sense) calculations described here with the computational results of Paper 4 appears to validate our understanding of the LLNL model and its application to simulation of the ODTX experiments.

A logical next step is to apply the reaction mechanism, with additions and adaptations as necessary, to other experimental scenarios, *e.g.*, cookoff, burning rate measurements, etc. The mechanism appears to have at least one obvious shortcoming: Apparently, all species are considered to occupy each volume element completely. In reality, at sufficiently fine spatial resolution, a volume element must contain either solids (HMX and/or fragments) or gases. Trapping of intermediate gases in solid pores may well lead to important effects; the mechanism clearly does not account, at least directly, for such effects.

References

(1) Catalano, E.; McGuire, R.; Lee, E.; Wrenn, E.; Ornellas, D.; Walton, J. In *Sixth Symposium (International) on Detonation*; Office of Naval Research ACR-221: Coronado, CA, 1976; pp 214-222.

(2) Tarver, C. M.; McGuire, R. R.; Lee, E. L.; Wrenn, E. W.; Brein, K. R. In *Seventeenth Symposium (International) on Combustion*; The Combustion Institute: Pittsburgh, 1978; pp 1407-1413.

(3) McGuire, R. R.; Tarver, C. M. In *Seventh Symposium (International) on Detonation*; Naval Surface Weapons Center NSWC MP 82-234: Annapolis, 1981; pp 56-64.

(4) Tarver, C. M.; Chidester, S. K.; Nichols, A. L. *J. Phys. Chem.* **1996**, *100*, 5794-4799.

(5) Nichols, A. L., III; Westerberg, K. W. *Numer. Heat Transfer, Part B* **1993**, *24*, 489-509.

(6) Becker, M. *Heat Transfer*; Plenum: New York, 1986.

TABLE 1: Thermal and Chemical Kinetic Parameters for HMX (LX-10)

(from Tarver *et al.*[4])

1. Thermal Properties of the Various Species

property	HMX	fragments	gases 1	gases 2
density (g/cm^3)	1.865			
heat capacity (cal/g-K) at				
293 K	0.24	0.22	0.24	0.27
433 K	0.34	0.31	0.27	0.28
533 K	0.40	0.36	0.29	0.29
623 K	0.46	0.42	0.31	0.30
773 K	0.55	0.50	0.35	0.31
>1273 K	0.55	0.50	0.42	0.35
thermal conductivity (cal/cm-s-K) at				
293 K	1.23×10^{-3}	6.50×10^{-4}	1.0×10^{-4}	1.0×10^{-4}
433 K	9.70×10^{-4}	5.00×10^{-4}	1.0×10^{-4}	1.0×10^{-4}
533 K	8.10×10^{-4}	4.00×10^{-4}	1.0×10^{-4}	1.0×10^{-4}
>633 K	7.00×10^{-4}	3.00×10^{-4}	1.0×10^{-4}	1.0×10^{-4}
heat of formation at 298 K (cal/g)				
	+61.0	+161.0	–139.0	–1339.0

2. Chemical Kinetic Parameters

HMX → fragments → intermediate gases → final gases

reaction number	1	2	3
ln frequency factor (s^{-1})	48.7	37.3	28.1
activation energy (kcal/m)	52.7	44.1	34.1
order of reaction	1	1	2
heat of reaction at 298 K (cal/g)	+100	–300	–1200

TABLE 2: Formation Reactions of the Various Species

Species	ΔN_g
HMX	
$4\ C(s) + 4\ H_2(g) + 4\ N_2(g) + 4\ O_2(g) \rightarrow C_4H_8N_8O_8(s)$	–12
Fragments	
$C(s) + H_2(g) + N_2(g) + O_2(g) \rightarrow CH_2N_2O_2(s)$	–3
Gases 1	
$CH_2O + N_2O$:	
C(s) + H2(g) +1/2 O2(g) Æ CH2O(g)	–1/2
$N_2(g) + 1/2\ O_2(g) \rightarrow N_2O(g)$	–1/2
Average	–1/2
$HCN + HNO_2$:	
$1/2\ H_2(g) + C(s) + 1/2\ N_2(g) \rightarrow HCN(g)$	0
$1/2\ H_2(g) + 1/2\ N_2(g) + O_2(g) \rightarrow HNO_2(g)$	–1
Average	–1/2
Gases 2	
$H_2O + CO + N_2$:	
$H_2(g) + 1/2\ O_2(g) \rightarrow H_2O(g)$	–1/2
$C(s) + 1/2\ O_2(g) \rightarrow CO(g)$	1/2
$N_2(g) \rightarrow N_2(g)$	0
Average	0
$H_2 + CO_2 + N_2$:	
$H_2(g) \rightarrow H_2(g)$	0
$N_2(g) \rightarrow N_2(g)$	0
$C(s) + O_2(g) \rightarrow CO_2(g)$	0
Average	0

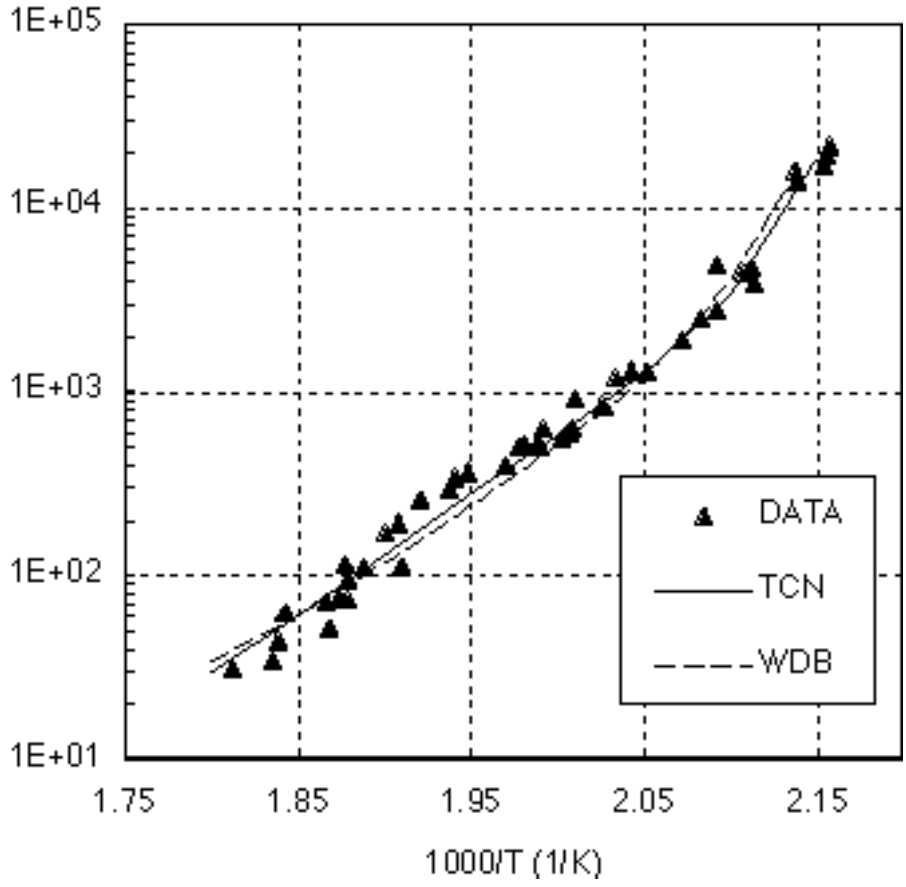

Figure 1. Time to explosion for HMX shperes of 1.27 cm diameter. Triangles and the solid line are experimental and computational results, respectively, from Fig. 1 of Tarver *et al.*[4] (Paper 4). The dashed line results from calculations described in the text.

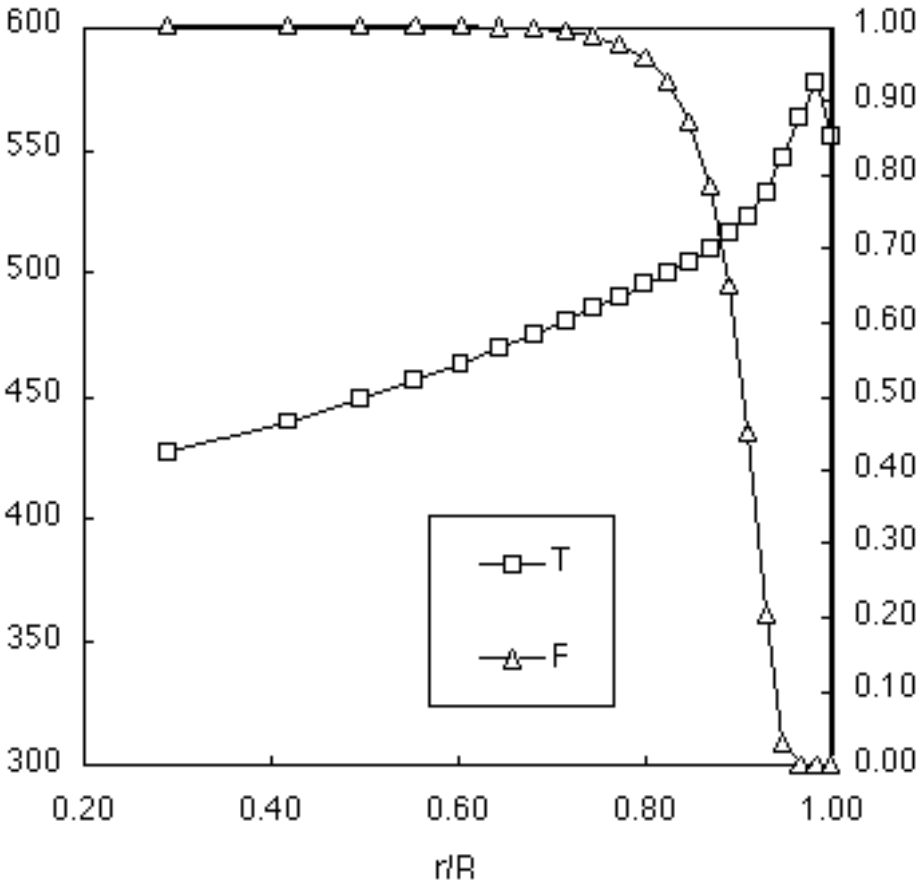

Figure 2. Radial profiles of temperature and HMX mass fraction at the time of "explosion," calculated as described in the text for $1000/T_S = 1.80$ ($T_S = 556$ K).

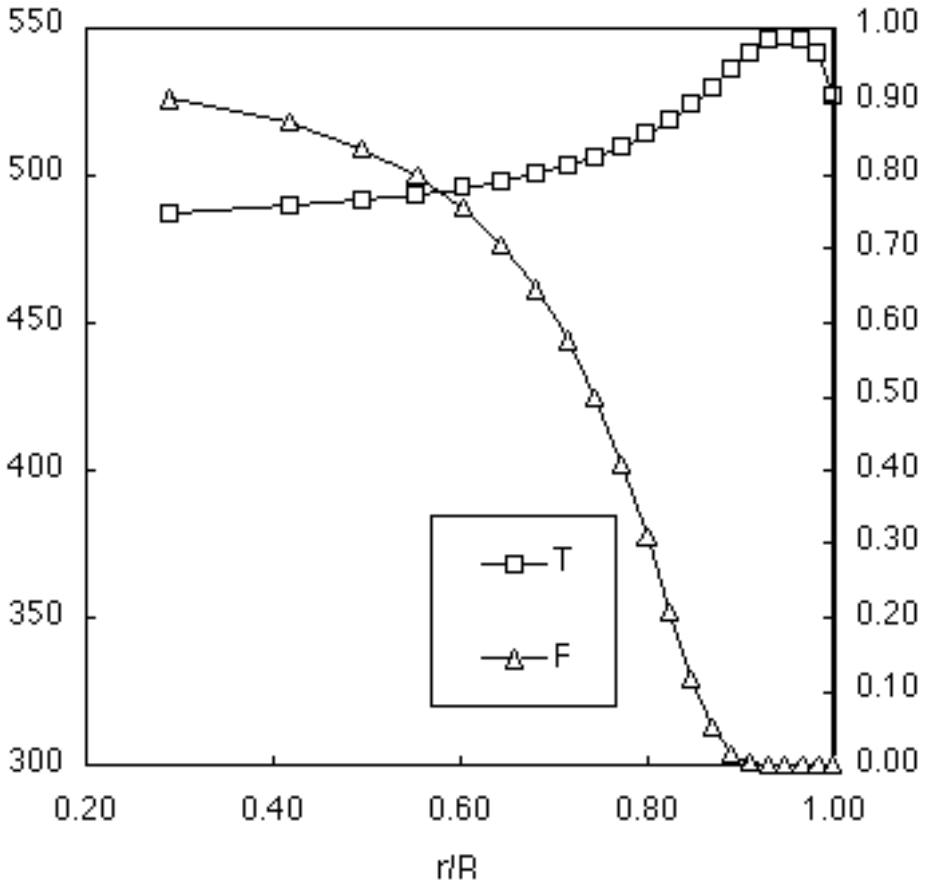

Figure 3. Radial profiles of temperature and HMX mass fraction at the time of "explosion," calculated as described in the text for $1000/T_S = 1.90$ ($T_S = 526$ K).

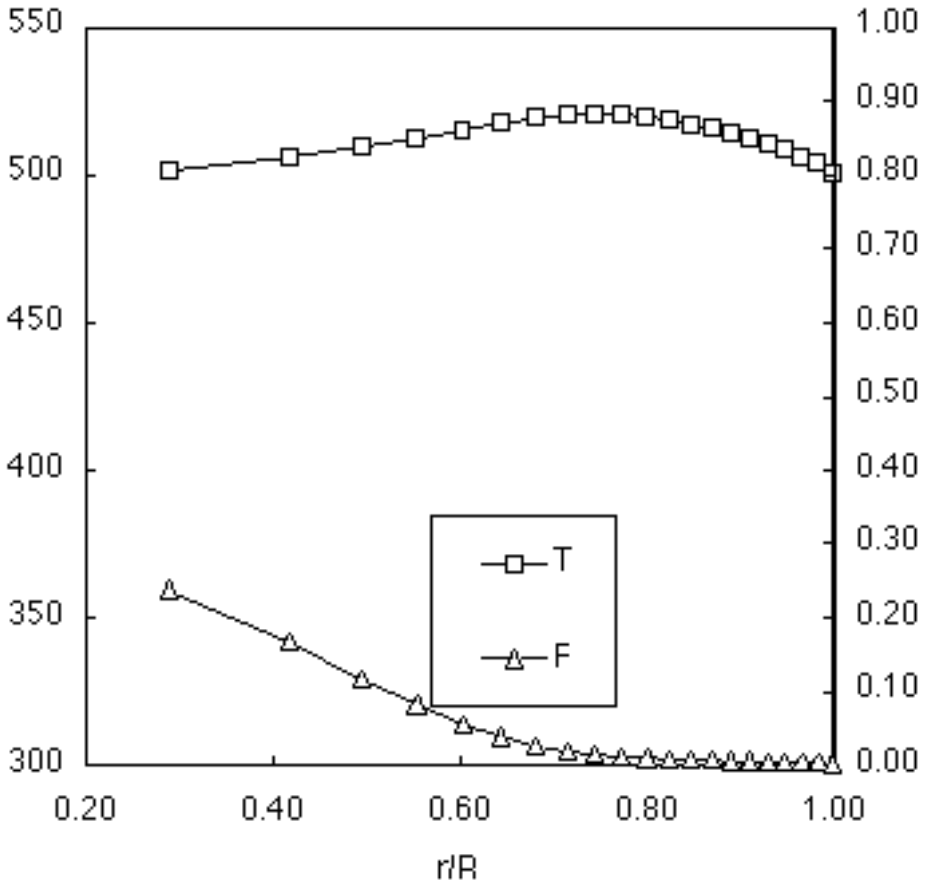

Figure 4. Radial profiles of temperature and HMX mass fraction at the time of "explosion," calculated as described in the text for $1000/T_S = 2.00$ ($T_S = 500$ K).

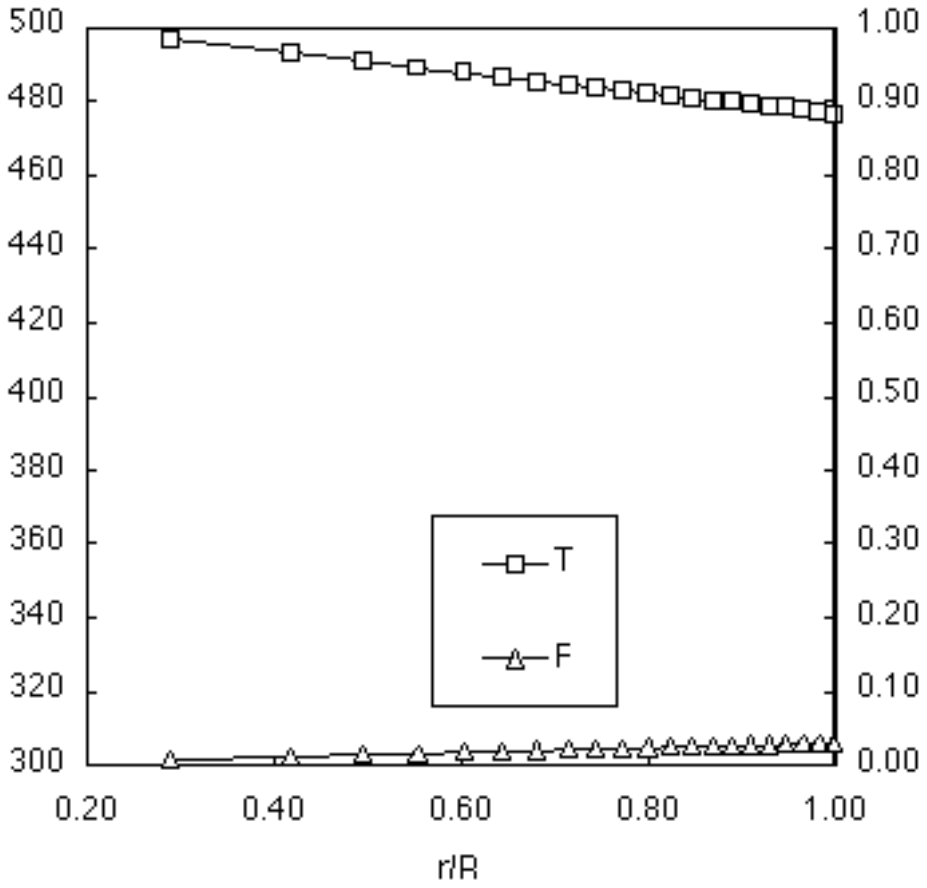

Figure 5. Radial profiles of temperature and HMX mass fraction at the time of "explosion," calculated as described in the text for 1000/Ts = 2.10 (Ts = 476 K).

Copies to:
Blaine Asay, DX-2, MS C920
David Funk, DX-2, MS C920
Steve Son, DX-2, MS C920
Peter Dickson, DX-2, MS G755
Bob Sander, CST-4, MS E543
Brian Henson, CST-6, MS J567
John Lyman, CST-6, MS J567
Richard Oldenborg, CST-6, MS J567
Dave Zerkle, CST-6, MS J567